High Efficiency Solution-Processed Organic Light-Emitting Diodes with Tetradentate Platinum(II) Emitters

Gang Cheng,[§,†] *Yoonhyun Kwak*,[‖] *Wai-Pong To*,[§,†] *Tsz-Lung Lam*,[†] *Glenna So-Ming Tong*,[†] *Man-Ki Sit*,[†] *Shaolong Gong*,[‡] *Byoungki Choi*,[‖] *Wha il Choi*,[⊥] *Chuluo Yang*,[*,‡] *Chi-Ming Che*[*,§,†]

[§]*HKU Shenzhen Institute of Research and Innovation, Shenzhen 518053, P. R. China*

[†]*State Key Laboratory of Synthetic Chemistry, HKU-CAS Joint Laboratory on New Materials, and Department of Chemistry, The University of Hong Kong, Pokfulam Road, Hong Kong SAR, China.*

[‖]*Samsung Electronics, Organic Material Lab，SAIT, 130 Samsung-ro, Yeongtong-gu, Suwon-si, Gyeonggi-do, 16678, Korea*

[‡]*Hubei Key Lab on Organic and Polymeric Optoelectronic Materials, Department of Chemistry, Wuhan University, Wuhan, 430072, P. R. China*

[⊥]*Samsung Electronics, Samsung Research Funding & Incubation Center for Future Technology Seoul R&D Campus, Umyeon dong 33, Seongchon-gil, Seocho-gu, Seoul, 06765, Korea*

KEYWORDS: organic light-emitting diodes; platinum complexes; solution-process; bipolar organic host

ABSTRACT: The realization of high efficiency solution-processed organic light-emitting diodes (OLEDs) by using phosphorescent tetradentate Pt(II) emitters and bipolar organic hosts is demonstrated in this work. To investigate the effect of organic host on the platinum dopant, the performances of solution-processed Pt-OLEDs with various combination between four tetradentate Pt(II) emitters, including two newly developed **tetra-Pt-S2** and **tetra-Pt-S3**, and three bipolar organic hosts **m-TPAPy**, **o-TPAPy**, and **o-CzPy**, have been analyzed and compared. Among the tetradentate Pt(II) complexes studied in this work, **tetra-Pt-S3** exhibited the best electroluminescent performance attributable to its bulky molecular scaffold structure, high emission quantum yield, and good solubility in common organic solvents. High external quantum efficiencies (EQEs) of up to 22.4% were achieved in the solution-processed OLED with **tetra-Pt-S3** emitter and **m-TPAPy** host at the dopant concentration of 4 wt%. At a high luminance of 1000 cd m^{-2}, the EQE of this device decreased slightly to 21.0%.

INTRODUCTION

Efficient solution-processed organic light-emitting diodes (OLEDs) were first demonstrated by Friend and co-workers by using poly (*p*-phenylene vinylene) (PPV) conjugated polymer as emitter almost three decades ago.[1] Owing to easy fabrication, light weight, and capability of building on flexible substrates, this kind of device has potential application in flexible and low-cost displays, such as electronic paper and bendable displays that can be integrated into curved surfaces. However, the performance of early solution-processed OLEDs was limited by the fluorescence nature of conjugated organic polymers,[2-4] as only singlet excitons can emit light while triplet ones are wasted due to inefficient spin-orbit coupling.[5, 6] In this regard, thermally activated delayed fluorescent (TADF) emitters and phosphorescent metal complexes have been

extensively studied and used to fabricate solution-processed OLEDs as both singlet and triplet excitons can be utilized.[7-22] Among the various phosphorescent emitters reported in the literature, only Ir(III) complexes have been intensively studied as the emitting dopant in solution-processed OLEDs.[16] These complexes have been physically or chemically dispersed in conjugated polymers or small molecular hosts to construct the emitting layer (EML) of solution-processed OLEDs.[12-14, 17-22] High EQEs of up to 28.5%, 29% and 28.5% have been achieved in red, green and white single-cell light-emitting devices, respectively.[21, 22] Kido and co-workers reported a high EQE of 28% at a high luminance of 5000 cd m^{-2} in tandem solution-processed OLEDs.[11] Nonetheless, research on the use of other efficient metal phosphors, such as platinum (II) complexes,[23-26] as an emitting dopant in solution-processed OLEDs is in its infancy.[25, 27-29] As Pt(II) emitters usually adopt planar molecular structure, it is envisioned that the horizontal dipole ratio could be higher, which is beneficial to higher out-coupling efficiency. In addition, due to the inherent coordination geometry, Pt(II) ion can form complexes with a single chelating tetradentate ligand that have extra thermal stability and slower non-radiative decay rate when compared with complexes with multiple chelating ligands. For instance, our previously reported **tetra-Pt-N** and **tetra-Pt-S1** are thermally stable with high photoluminescence quantum yield (PLQY).[26]

Recently, bipolar organic compounds containing both electron-donating and electron-accepting functionalities have been utilized as the host for Ir(III) complexes in solution-processed OLEDs that were found to give better device performance when compared with those of devices with a polymer host.[30-34] The superior performance of solution-processed OLEDs with a bipolar organic host is attributable to the balanced charge-transporting property and higher T_1 of these organic molecules.[35] Although **tetra-Pt-N** and **tetra-Pt-S1** have been reported to exhibit high EQEs of up to 27.6% in vacuum-deposited OLEDs,[26] there has been no report on their application in solution-processed devices. In the present work, their EL

performances were also evaluated in solution-processed OLEDs. Two new structurally similar emitters, **tetra-Pt-S2** and **tetra-Pt-S3** (Chart 1), have also been synthesized and their photo-physical properties in both solution and thin film states were investigated herein. The major structural difference between **tetra-Pt-S2** and **tetra-Pt-S1** is the presence of a CR_2-bridge that fuses the O^N moiety of the tetradentate ligand scaffold in the former which increases the rigidity of the O^N^C^N ligand which, in principle, should further retard the non-radiative rate, thus boosting the PLQY. Previously reported **tetra-Pt-N** has a higher PLQY than **tetra-Pt-S1** in CH_2Cl_2 solution and it was speculated that the more electron-donating phenylimido spiro-linkage may be the reason for its higher PLQY as compared with the **tetra-Pt-S1** with fluorene spiro-linkage. **tetra-Pt-S3** was thus synthesized with the fluorene ring in **tetra-Pt-S1** replaced by a more electron-donating xanthene spiro-linkage. These four Pt(II) complexes (Chart 1) were also respectively doped into three bipolar organic hosts to fabricate solution-processed OLEDs. The three bipolar organic hosts used in this work have been employed as host materials for phosphorescent blue emitters in vacuum-deposited OLEDs and displayed decent device performances,[36, 37] while they have not been utilized as the host in solution-processed OLEDs yet. A maximum EQE of 22.4% and a maximum luminance of almost 40000 cd m^{-2} have been achieved in the device with **tetra-Pt-S3** emitter and **m-TPAPy** host. PL properties of various combinations of the four tetradentate Pt(II) emitters and the three organic hosts have also been investigated.

RESULTS AND DISCUSSION

The structure of the four phosphorescent [Pt(O^N^C^N)] complexes that were studied in this work as emitting dopants for solution-processed OLEDs are depicted in **Chart 1**. In previous works,[26] **tetra-Pt-N** and **tetra-Pt-S1** have been reported as efficient phosphorescent emitters in vacuum-deposited OLEDs; while **tetra-Pt-S2** and **tetra-Pt-S3** are new compounds. As

depicted in **Chart 2**, three bipolar organic molecules **m-TPAPy**, **o-TPAPy**, and **o-CzPy** were used as host for these Pt(II)-emitters. The bipolar transporting property of these three organic molecules originates from the combination of a pyridine electron acceptor and carbazole (as in **o-CzPy**) or triphenylamine (as in **o-TPAPy** and **m-TPAPy**) electron donor.[36, 37] The energy levels of these three molecules are listed in **Table S1**.

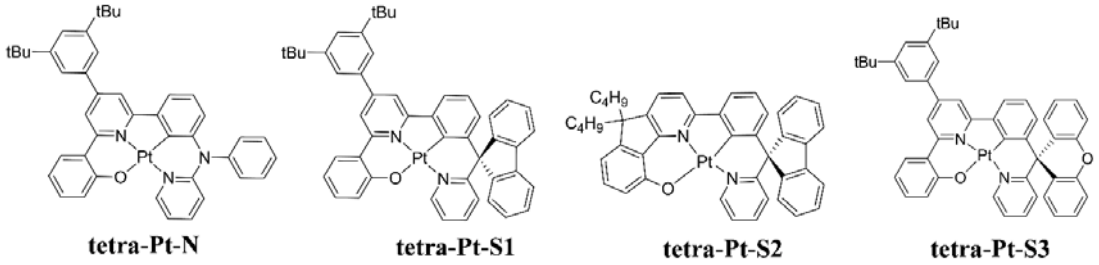

Chart 1. Chemical structures of [Pt(O^N^C^N)] complexes used in this work.

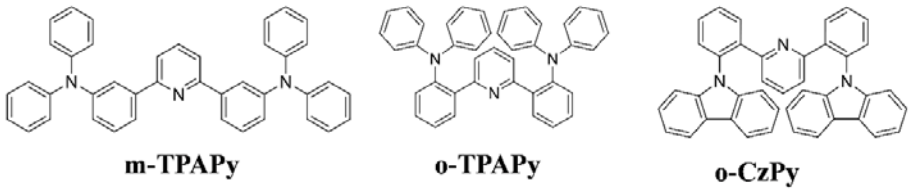

Chart 2. Chemical structures of host molecules in this work.

The synthetic procedures for these complexes are given in the **Supporting Information**. Similar to the synthesis of **tetra-Pt-S1**, the spiro-fluorene and xanthene units of **tetra-Pt-S2** and **tetra-Pt-S3** were prepared *via* Grignard reactions and subsequent cyclization in acid while the construction of substituted pyridine units was accomplished by Kröhnke annulation.[26] Metalation was realized by a one-pot cyclometallation reaction of the [O^N^C^N] ligand with K_2PtCl_4 in refluxing glacial acetic acid and chloroform (v/v = 9/1) mixture. The crude reaction mixture was purified by flash column chromatography on silica gel (SiO_2) using hexane and dichloromethane mixture as eluent. Light yellow crystalline complexes were obtained *via* further purification by sublimation at 380 °C under 1×10^{-5} Torr with yields of sublimation

>50%. As revealed from thermogravimetric analysis curves (TGA) depicted in **Figure S5**, both **tetra-Pt-S2** and **tetra-Pt-S3** display high thermal stability with decomposition temperature, T_d, of over 380 °C. Meanwhile, both Pt(II) complexes are stable toward air and moisture and show good solubility in common organic solvents, allowing them to be used in solution-processed OLEDs.

The crystal structure of **tetra-Pt-S2** complex is depicted in **Figure 1**. The Pt atom adopts a distorted square-planar geometry with C24−Pt1−N2 angle of 81.4(2)°. The pyridine unit adjacent to the spiro-carbon atom deviates from the mean ligand plane by 4.6°, presumably due to the presence of an sp^3 C-bridge of spiro-fluroene moiety. The N2−Pt1−N1 angle deviates from the ideal angle of 180° with a value of 172.2(2)°, which is much larger than those of the reported [Pt(O^N^C^N)] or [Pt(N^C^N)Cl] complexes. This would result in a smaller ring strain, as the incorporation of spiro-fluorene in the tetradentate ligand scaffold gives a 6−5−6 membered metallacycle. The Pt1−N1, Pt1−N2, Pt1−O1, and Pt1−C24 distances are respectively 2.037, 1.977, 2.107 and 1.954 Å, being comparable to those of reported [Pt(N^C^N)Cl] and [Pt(O^N^N)Cl] complexes.[38-40] The **tetra-Pt-S2** molecules align in a head-to-tail manner with a Pt-Pt separation of 7.089 Å [see **Figure S7**], similar to that of the structurally related **tetra-Pt-S1** but is significantly longer than those of reported [Pt(O^N^C^N)] complexes (~3.2–3.4 Å) which have no spiro-linkage.[41] The intermolecular π–π separation between the ligand planes is approximately 3.9 Å implying negligible or weak π–π interaction. The intermolecular π–π separation of **tetra-Pt-S2** is slightly longer than the interplanar distance of 3.6 Å observed in the molecular packing of **tetra-Pt-N** in which the complex molecules are also aligned in a head-to-tail manner.[26] The spiro-fluorene of **tetra-Pt-S2** was found to orientate vertically above the mean plane of the adjacent **tetra-Pt-S2** complex molecule, which may account for the slightly longer intermolecular π–π separation of **tetra-Pt-S2**.

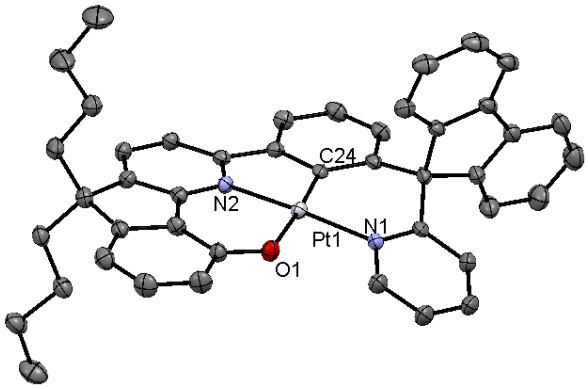

Figure 1. Perspective view of **tetra-Pt-S2**. The thermal ellipsoids are at 30 % probability level. All hydrogen atoms and solvent molecules have been omitted for clarity.

The electrochemical properties of **tetra-Pt-N** and **tetra-Pt-S1** have been reported in our previous work[26] and those of **tetra-Pt-S2** and **tetra-Pt-S3** were investigated in this study by cyclic voltammetry in DMF containing 0.1 M $^{n}Bu_4NPF_6$ as supporting electrolyte. The data are shown in **Table S5**. As depicted in **Figure S8**, Both **tetra-Pt-S2** and **tetra-Pt-S3** show one irreversible oxidation wave with E_{pa} at +0.65 to +0.63 V vs $FeCp_2^{+/0}$, respectively, and one quasi-reversible reduction couple with $E_{1/2}$ value of −2.40 V for **tetra-Pt-S2** and −2.22 V for **tetra-Pt-S3**. These reduction couples are largely attributed to ligand centered reduction and their oxidation waves are assigned as oxidation of Pt(II) to Pt(III).

The photo-physical data of **tetra-Pt-S2** and **tetra-Pt-S3** are given in **Table 1**. The UV-vis absorption spectra of **tetra-Pt-S2** and **tetra-Pt-S3** are depicted in **Figure 2**. The intense absorption bands at 250–320 nm with absorptivity in the order of 10^4 mol^{-1} dm^3 cm^{-1} are assigned to $^1\pi$-π^* transitions localized on the O^N^C^N ligand.[26] According to previous works, the lower energy (λ > 370 nm), less intense absorption bands ($\varepsilon < 10^4$ mol^{-1} dm^3 cm^{-1}) are assigned to an admixture of metal-to-ligand charge transfer (MLCT) and intraligand (IL) transitions. As listed in **Table 1**, **tetra-Pt-S2** and **tetra-Pt-S3** exhibit intense green and yellow photoluminescence respectively in degassed CH_2Cl_2 at room temperature with quantum yield of 59% and 71%, respectively. **Tetra-Pt-S3** displays a structure-less broad emission band with

peak maximum at 516 nm and emission lifetime of 6.0 μs, similar to those of **tetra-Pt-S1** which share the same Pt(O^N^C^N) skeleton (λ_{em} = 517 nm, τ = 5.1 μs),[26] indicating that both **tetra-Pt-S1** and **tetra-Pt-S3** have similar emissive excited state. According to the previous DFT/TDDFT calculations,[26] the emission of **tetra-Pt-S3** in CH_2Cl_2 solution is derived from ^{3}ILCT $\rightarrow$ S_0 (ILCT = intraligand charge transfer. On the other hand, **tetra-Pt-S2** shows a vibronic-structured emission band peaked at 499 nm with vibronic progressions of ~1400 cm^{-1}. Concomitantly, the emission lifetime is markedly lengthened to 36.4 μs, pointing to a distinctly different emissive excited state with emission profile that is consistent with a ^{3}LC $\rightarrow$ S_0 transition (LC = ligand centred). Indeed, as summarized in **Table S2**, the radiative decay rate constant, k_r, of **tetra-Pt-S2** (1.6×10^4 s^{-1}) is an order of magnitude smaller than those of other complexes investigated in this work ($1.2-2.1 \times 10^5$ s^{-1}). The change in the nature of emissive excited state upon fusing the O^N moiety with C-bridge has also been found in previous works.[26, 39] In addition, the steric hindrance imposed by the spiro unit effectively suppresses bimolecular interactions.[42] The self-quenching rate constant, k_q, of **tetra-Pt-S2** and **tetra-Pt-S3** are in the order of 10^6-10^7 mol^{-1} dm^3 s^{-1} (see **Table 1**), both of which are smaller than those of reported [Pt(O^N^C^N)] complexes.[24, 25, 41] In comparison, **tetra-Pt-S2** shows a much lower k_q than that of **tetra-Pt-S3** (*i.e.*, 6.7×10^6 *vs.* 5.7×10^7 $mol^{-1}dm^3s^{-1}$), probably due to the presence of two long butyl chains on the C-bridge that further restricts intermolecular interaction.

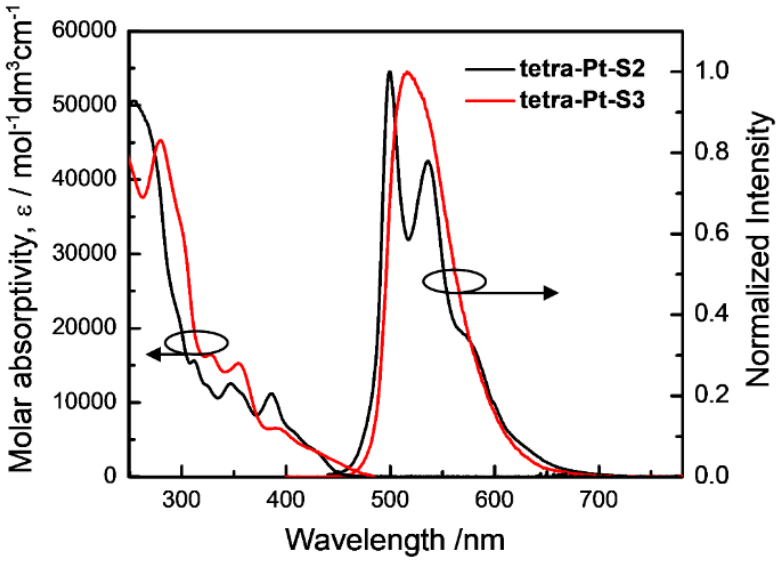

Figure 2 UV-visible absorption and emission spectra of **tetra-Pt-S2** and **tetra-Pt-S3** in degassed CH_2Cl_2 (concentration of 2×10^{-5} M) at 298 K.

Table 1. Photophysical data of **tetra-Pt-S2** and **tetra-Pt-S3**

Complex	UV-Vis absorption, λ_{abs}[a] [nm] ($\varepsilon \times 10^4$ [mol^{-1} dm^3 cm^{-1}])	Emission			
		λ_{max}[a] [nm]; τ [μs] in solution	λ_{max} [nm] in film	Φ_{em} in solution[b]; Φ_{em}[c] in film	k_q [d][mol^{-1} dm^3 s^{-1}]
tetra-Pt-S2	255 (5.1), 269 (sh, 4.7), 297 (sh, 2.2), 313 (1.6), 325 (sh, 1.2), 348 (1.3), 361 (sh, 1.1), 388 (1.1), 427 (sh, 0.37)	499, 536, 580 (sh); 36.4	501, 537, 575 (sh)	0.59; 0.40	6.7×10^6
tetra-Pt-S3	280 (4.5), 302 (sh, 3.3), 329 (1.6), 355 (1.5), 394 (0.65), 427 (sh, 0.35)	516, 537 (sh); 6.0	516, 530, 582 (sh)	0.71; 0.70	5.7×10^7

[a]Determined in degassed CH_2Cl_2 at a concentration of 2×10^{-5} mol dm^{-3}. [b]Emission quantum yield was estimated with $[Ru(bpy)_3](PF_6)_2$ (bpy = 2,2'-bipyridine) in degassed CH_3CN as a standard with $\Phi_{em} = 0.062$. [c]5 wt% in PMMA film; determined with Hamamatsu C11347 Quantaurus-QY Absolute PL quantum yield measurement system. [d]Emission self-quenching rate constant.

The solvent effect on the absorption and emission of these complexes has been examined. The results are depicted in **Figure 3**, and the data are summarized in **Table 2**. In general, the lowest energy absorption band of these four complexes show a slight blue-shift (< 10 nm) upon changing the solvent polarity. On the other hand, **tetra-Pt-N**, **tetra-Pt-S1**, and **tetra-Pt-S3**, which do not

have the O^N rings fused, display discernible red shift in emission maximum upon changing solvent polarity. For example, for **tetra-Pt-S3**, λ_{em} shifts from 514 nm (toluene) to 533 nm (CH_3CN), corroborating the assignment of the emissive excited state being charge transfer in nature. On the contrary, changing the solvent polarity has little effect (~ 2 nm) on the emission maximum of **tetra-Pt-S2**, which is consistent with the emission assignment of being derived from a ^{3}LC excited state.

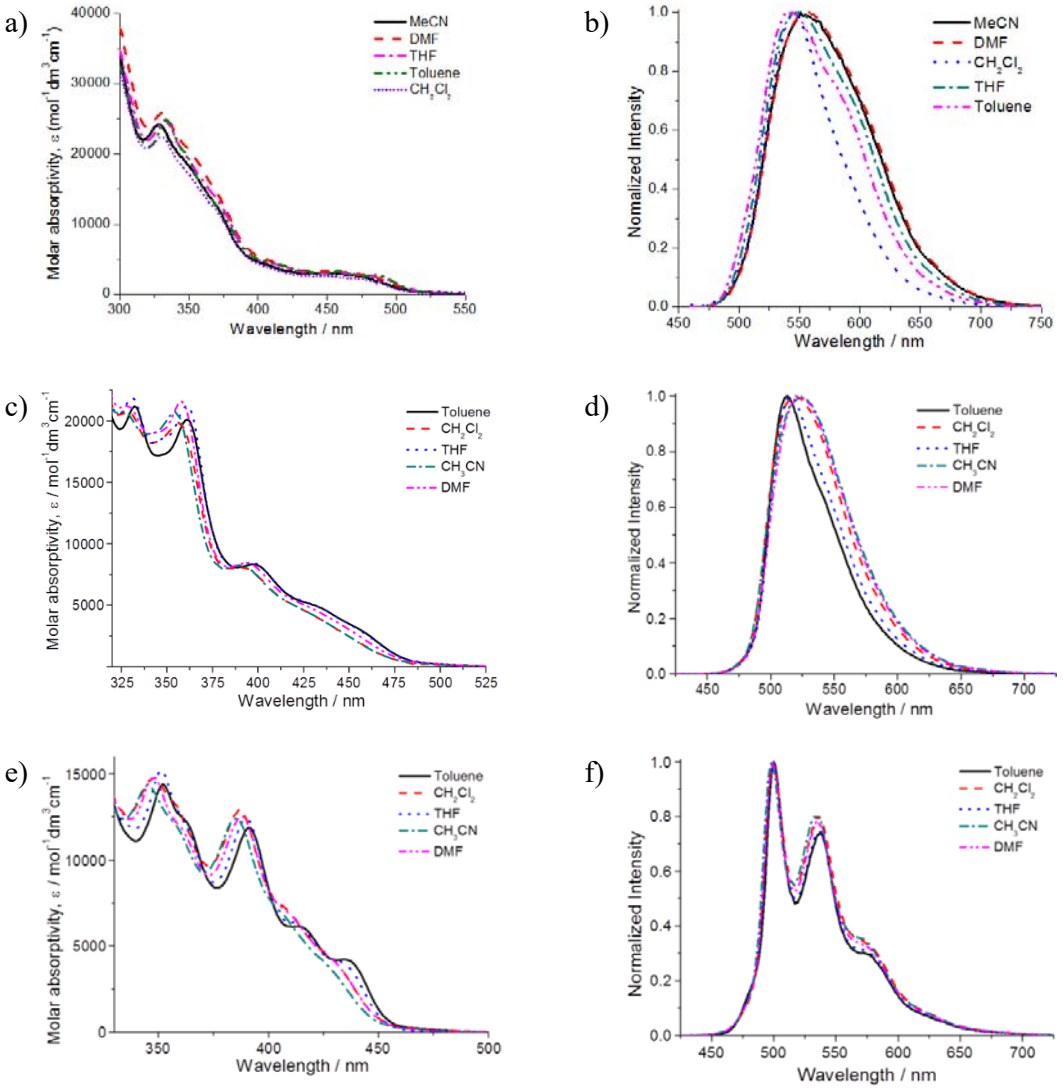

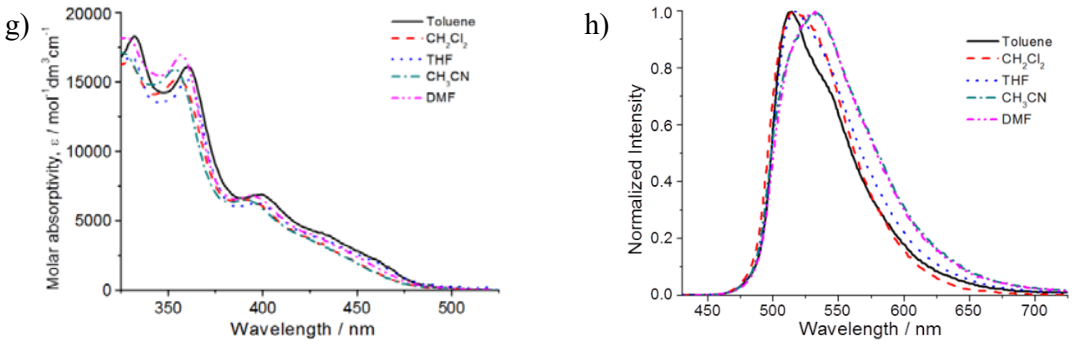

Figure 3. (a, c, e, g) UV-vis absorption spectra and (b, d, f, h) emission spectra of **tetra-Pt-N**, **tetra-Pt-S1**, **tetra-Pt-S2** and **tetra-Pt-S3** (concentration = 2×10^{-5} M) respectively in different solvents.

Table 2. Photo-physical data of the Pt(II) complexes in different solvents at room temperature (2×10^{-5} mol dm^{-3}).

Complex	Solvent	UV-Vis absorption, λ_{abs} / nm[a] (ε / 10^4 mol^{-1} dm^3 cm^{-1})	Emission	
			λ_{max} / nm; τ / μs	Quantum Yield, Φ_{em}[b]
tetra-Pt-N	Toluene	334 (2.5), 350 (1.9), 372 (sh, 1.2), 458 (sh, 0.32), 485 (sh, 0.28)	538; 4.6	0.69
	CH_2Cl_2	330 (2.2), 350 (1.9), 370 (sh, 1.1), 450 (sh, 0.27), 481 (sh, 0.21)	551; 4.3	0.90
	THF	332 (2.5), 350 (1.9), 372 (sh, 1.3), 457 (sh, 0.32), 484 (sh, 0.25)	549; 5.0	0.69
	CH_3CN	328 (2.4), 348 (1.9), 370 (sh, 1.3), 451 (sh, 0.31), 484 (sh, 0.20)	551; 5.4	0.53
	DMF	331 (2.6), 355 (1.9), 376 (sh, 1.2), 452 (sh, 0.33), 483 (sh, 0.25)	556; 4.8	0.59
tetra-Pt-S1	Toluene	332 (2.1), 361 (2.0), 397 (0.83), 442 (sh, 0.41)	513, 543; 4.7	0.93
	CH_2Cl_2	329 (2.1), 356 (2.0), 391 (0.81), 439 (sh, 0.34)	520; 5.1	0.77
	THF	331 (2.2), 361 (2.1), 396 (0.85), 436 (sh, 0.47)	516; 5.2	0.95
	CH_3CN	326 (2.1), 354 (2.1), 390 (0.82), 432 (sh, 0.41)	525; 6.0	0.78
	DMF	328 (2.1), 358 (2.2), 394 (0.84), 438 (sh, 0.41)	522; 4.7	0.79
	Toluene	352 (1.4), 363 (sh, 1.2), 391 (1.2), 412 (0.61), 436 (sh, 0.42)	500, 538, 578 (sh); 33.1	0.73
	CH_2Cl_2	348 (1.5), 359 (sh, 1.3), 387 (1.3), 409 (sh, 0.71), 433 (sh, 0.37)	500, 537, 581 (sh); 36.4	0.59

tetra-Pt-S2	THF	351 (1.5), 361 (sh, 1.2), 390 (1.2), 412 (sh, 0.64), 435 (sh, 0.39)	500, 537, 579 (sh); 38.9	0.75
	CH_3CN	345 (1.4), 358 (sh, 1.2), 385 (1.2), 407 (sh, 0.68), 425 (sh, 0.41)	498, 534, 578(sh); 32.5	0.56
	DMF	348 (1.5), 360 (sh, 1.2), 388 (1.3), 410 (sh, 0.68), 430 (sh, 0.41)	499, 536, 580 (sh); 22.4	0.46
	Toluene	332 (1.8), 361 (1.6), 399 (0.69), 432 (sh, 0.41)	514; 4.9	0.70
	CH_2Cl_2	329 (1.6), 355 (1.5), 394 (0.65), 427 (sh, 0.35)	516; 6.0	0.71
tetra-Pt-S3	THF	330 (1.7), 361 (1.6), 399 (0.69), 432 (sh, 0.41)	516; 5.4	0.72
	CH_3CN	326 (1.7), 353 (1.6), 391 (0.65), 432 (sh, 0.33)	533; 5.5	0.59
	DMF	328 (1.8), 357 (1.7), 394 (0.68), 431 (sh, 0.37)	532; 4.2	0.55

[a]Absorption from 325–500 nm. [b]Emission quantum yield was estimated with based on $[Ru(bpy)_3](PF_6)_2$ (bpy = 2,2'-bipyridine) in degassed CH_3CN as standard $\Phi_{em} = 0.062$.

Time-resolved emission spectra of these complexes are depicted in **Figure S6**. The emission profiles in CH_2Cl_2 remained unchanged throughout the decay process, indicating absence of excimeric emission. Time-resolved absorption (TA) spectra of these complexes in CH_2Cl_2 are also depicted in **Figure 4**. **Tetra-Pt-N**, **tetra-Pt-S1**, and **tetra-Pt-S3** display similar TA spectra with a sharp peak at λ_{max} ~385–395 nm and a broad absorption band covering 450–800 nm; the similarities in TA spectral profiles may likely be due to their similar Pt(O^N^C^N) scaffold with major difference only at the spiro-linkage, indicating that the emissive excited state does not have significant contributions from the spiro-linkage. On the contrary, **tetra-Pt-S2** shows distinctly different TA profile with a poorly-resolved absorption band at 410-500 nm and tails extending to $\lambda > 700$ nm. Their TA decay lifetimes are similar to their respective steady -state emission lifetimes, suggesting that these TA profiles originate from the emissive triplet excited states.

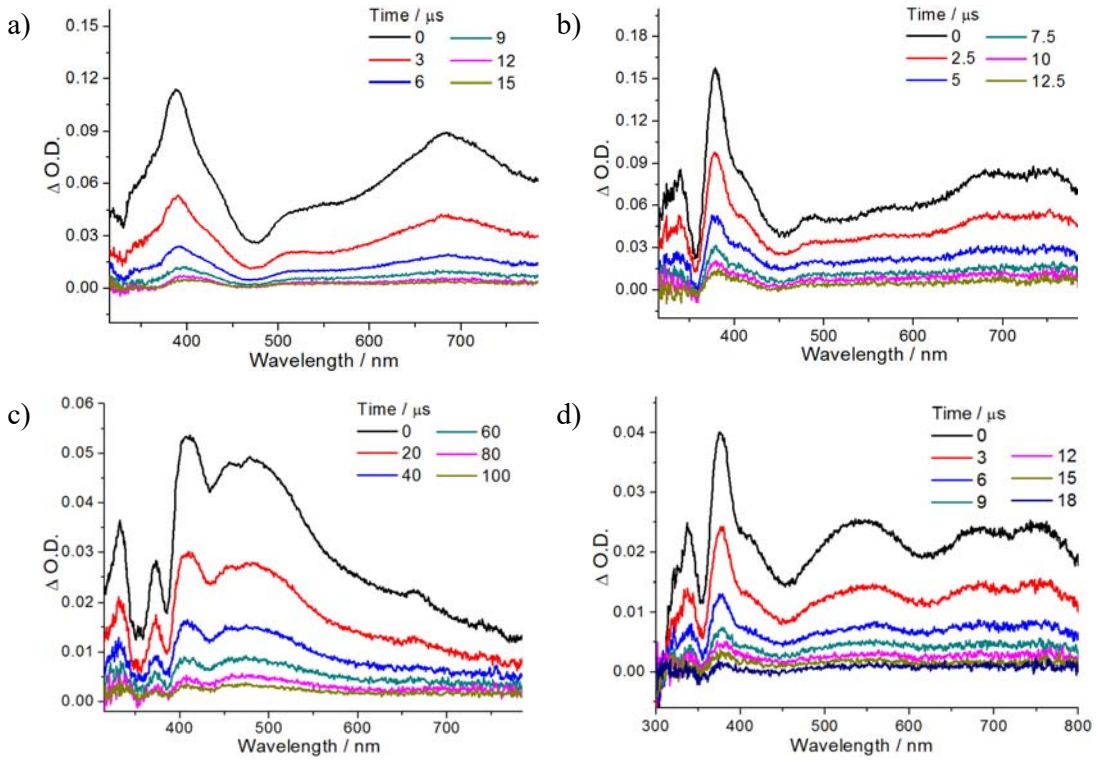

Figure 4. Time-resolved transient absorption spectra of a) **tetra-Pt-N**, b) **tetra-Pt-S1**, c) **tetra-Pt-S2** and d) **tetra-Pt-S3** (concentration = 2×10^{-5} M) respectively in CH_2Cl_2.

The photo-physical behavior of the four tetradentate Pt(II) complexes have also been investigated in thin films of **m-TPAPy**, **o-TPAPy**, and **o-CzPy**. **Tetra-Pt-N**, **tetra-Pt-S1,** **tetra-Pt-S2**, and **tetra-Pt-S3** are dispersed in thin films of **m-TPAPy**, **o-TPAPy**, and **o-CzPy** with a fixed dopant concentration of 12 wt%. The similarities in emission profiles and emission peak maximum in both solution and film state suggested that the nature of the emissive excited state does not change in the film state. It is notable that, except **tetra-Pt-S3**, the EL spectrum of the other three complexes investigated herein all are host-dependent; for instance, the emission maximum of the **tetra-Pt-S1** device slightly blue-shifted from 522 to 516 to 515 nm when the host was changed in succession from **m-TPAPy**, **o-TPAPy**, and **o-CzPy** possibly due to a change in polarity of the host and the host-guest interaction. High PLQYs of 0.71 and 0.84 are respectively achieved in the **m-TPAPy** thin films with **tetra-Pt-N** and **tetra-Pt-S3** dopants. On the other hand, host emission at around 420 nm was observed in the samples of

tetra-Pt-S1 and **tetra-Pt-S2** in **m-TPAPy** as depicted in **Figure S9**, leading to lower PLQYs in these samples (0.62 for **tetra-Pt-S1** and 0.22 for **tetra-Pt-S2)**. Such host emission could be the result of back energy transfer due to the relatively higher E_t of **tetra-Pt-S1** (2.49 eV) and **tetra-Pt-S2** (2.51 eV) and/or inefficient energy transfer from **m-TPAPy** (E_t=2.61 eV) to the emitters. By using **o-CzPy** (E_t=2.70 eV) to replace **m-TPAPy**, the host emission vanished in both samples of **tetra-Pt-S1** and **tetra-Pt-S2**, and their PLQYs were therefore augmented to 0.83 and 0.46, respectively.

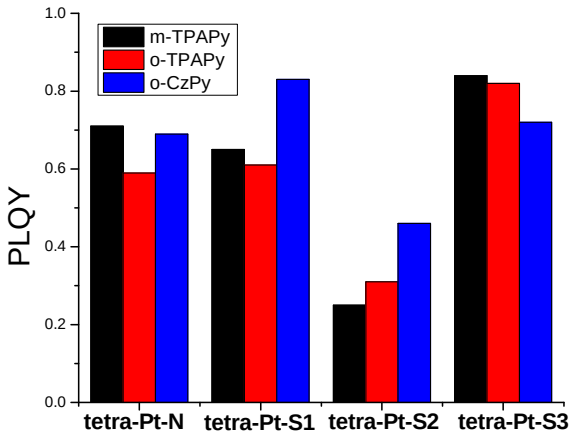

Figure 5. PLQY values of the Pt(II) complexes dispersed in different hosts with a fixed concentration of 12 wt%.

Solution-processed OLEDs with an architecture of ITO/PEDOT:PSS/Pt-emitter: host /TmPyPb/TPBi/LiF/Al were fabricated and characterized for examining the EL properties of the four tetradentate Pt(II) complexes in three different hosts of **m-TPAPy**, **o-TPAPy**, and **o-CzPy**. In these devices, TmPyPb [1,3,5-tri[(3-pyridyl)-phen-3-yl]benzene] was utilized as the hole-blocking layer (HBL) between the EML and the eletrcon-transporting layer of TPBi [2,2',2"-(1,3,5-benzinetriyl)-tris(1-phenyl-1-H-benzimidazole)].[25] The dopant concentration was fixed at 12 wt% for all devices. Normalized EL spectra of the four tetradentate Pt(II) complexes in different hosts are depicted in **Figure 6**. It is notable that the relative intensities

of the vibronic peaks in **tetra-Pt-S2** change in different hosts, with the $I_{0\text{-}1}/I_{0\text{-}0}$ ratio highest in **o-TPAPy** host and lowest in **o-CzPy** in the EL spectra. Since the $I_{0\text{-}1}/I_{0\text{-}0}$ ratio gives us clues on the extent of excited state structural distortion, it is interesting to note that structural distortion of **tetra-Pt-S2** in o-CzPy is being suppressed and it is probably the reason why the PLQY is the highest when doped in o-CzPy. Nevertheless, the EQEs of **tetra-Pt-S2** in all host materials are lower than those of the other Pt(II) complexes and suffer from pronounced efficiency roll-off at high luminance of 1000 cd m^{-2} due to its lower PLQY in thin films and longer emission lifetime of 36.4 μs in solution. We have also changed the dopant concentration of the **tetra-Pt-S1** devices with **m-TPAPy** and **o-CzPy** as hosts and the results are depicted in **Figure S12**. Increasing the dopant concentration leads to a slight red shift in the emission maximum and a concomitant broadening of the emission band attributed to the increase of the CT character in the emissive excited state at higher dopant concentration.

Table 3. Key EL performance data of **tetra-Pt-N**, **tetra-Pt-S1**, **tetra-Pt-S2**, and **tertra-Pt-S3**

EML	L_{max} [cd m^{-2}]	CE [cd A^{-1}]		PE [lm W^{-1}]		EQE [%]		CIE coordinates [(x, y)]
		Max	at 1000 cd m^{-2}	Max	at 1000 cd m^{-2}	Max	at 1000 cd m^{-2}	
m-TPAPy: **tetra-N**	32900	52.99	49.39	26.97	22.32	15.54	14.55	0.47, 0.53
o-TPAPy: **tetra-N**	14700	45.59	43.83	20.46	17.85	14.73	14.16	0.48, 0.51
o-CzPy: **tetra-N**	18500	53.04	42.65	22.22	15.19	16.83	13.53	0.48, 0.51
m-TPAPy: **tetra-S1**	26500	51.32	32.34	29.37	15.67	14.50	9.14	0.28, 0.65
o-TPAPy: **tetra-S1**	23750	53.21	36.67	25.72	14.25	14.63	10.02	0.32, 0.63
o-CzPy: **tetra-S1**	49600	59.42	57.09	27.24	22.42	16.63	15.99	0.29, 0.64
m-TPAPy: **tetra-S2**	1400	8.21	0.56	4.30	0.16	2.59	0.18	0.31, 0.59
o-TPAPy: **tetra-S2**	2450	6.46	1.81	2.90	0.50	2.10	0.59	0.35, 0.57
o-CzPy: **tetra-S2**	5970	12.12	7.58	5.07	2.93	3.89	2.62	0.28, 0.58
m-TPAPy: **tetra-S3**	28600	61.62	49.76	38.72	25.10	17.86	14.42	0.33, 0.62
o-TPAPy: **tetra-S3**	39800	55.11	48.44	27.65	19.92	15.78	13.87	0.31, 0.63
o-CzPy: **tetra-S3**	44950	50.99	50.76	20.07	19.02	14.78	14.71	0.30, 0.63

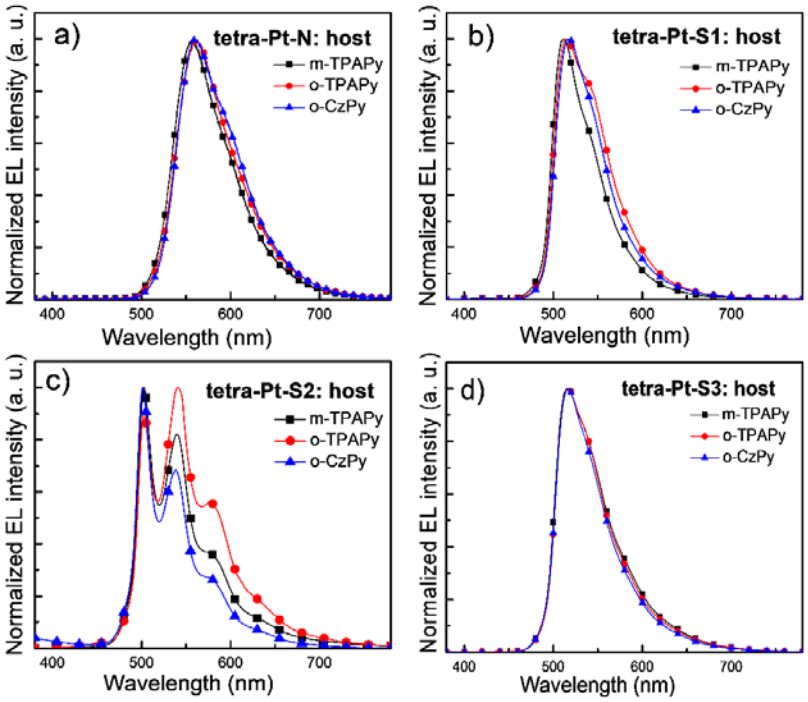

Figure 6. Normalized EL spectra of the OLEDs based on a) **tetra-Pt-N**, b) **tetra-Pt-S1**, c) **tetra-Pt-S2**, and d) **tetra-Pt-S3** in different hosts (**m-TPAPy**, **o-TPAPy**, and **o-CzPy**) with a fixed dopant concentration of 12 wt%.

EQE-luminance characteristics of the devices based on **tetra-Pt-N**, **tetra-Pt-S1**, **tetra-Pt-S2**, and **tetra-Pt-S3** in different hosts are depicted in **Figure 7**. Current density-luminance-voltage properties of these devices are shown in **Figures S8** and **S9**; corresponding key performance data are listed in **Table 3**. EQEs of the **tetra-Pt-S2** devices are much lower than those of the other devices due to the low PLQY of **tetra-Pt-S2** in thin films. High efficiencies of the devices based on **tetra-Pt-N**, **tetra-Pt-S1**, and **tetra-Pt-S3** in both **m-TPAPy** and **o-CzPy** hosts are attributed to the high PLQYs of these complexes in thin film state. Nonetheless, as depicted in **Figure S11**, the driving voltage of the devices with the **o-CzPy** host is higher than those with **m-TPAPy** ones. The high driving voltage of **o-CzPy** devices could be explained by its lower-lying HOMO energy level. As proposed in **Figure S13**, LUMO levels of both **m-TPAPy** and **o-CzPy** are 2.2 eV below vacuum level while the HOMO of **o-CzPy** is

lower than that of **m-TPAPy** by 0.3 eV, causing a higher energy barrier for the hole injection in **o-CzPy** devices and in turn increasing their driving voltage. Consequently, the power efficiency (PE) of **o-CzPy** devices is lower than that of the **m-TPAPy** devices, as listed in **Table 3**. From the perspective of energy cost and device long-term stability, **m-TPAPy** could be a better host for Pt-emitters studied in this work. To further understand the influence of different Pt(II) emitters upon the performances of **m-TPAPy** OLEDs, carrier balance and film morphology of the **m-TPAPy** film with different emitters were investigated with single carrier devices and atomic force microscopy (AFM) measurements. As shown in **Figure S16**, electron and hole current is balance for the **m-TPAPy** films with **tetra-Pt-N**, **tetra-Pt-S2** and **tetra-Pt-S3** when the driving voltage is higher than the turn-on voltage (~5 V) while the electron current is higher than hole current when **tetra-Pt-S1** was used as the dopant, leading to a relative lower EQE and pronounced efficiency roll-off of the **tetra-Pt-S1: m-TPAPy** device. AFM images of **m-TPAPy** films doped with **tetra-Pt-N**, **tetra-Pt-S1, tetra-Pt-S2,** and **tetra-Pt-S3** are shown in **Figure S17**. All **m-TPAPy** films display smooth morphologies, suggesting nearly even dispersion of dopants in the host for all Pt(II) complexes. Nonetheless, the lowest roughness of the **tetra-Pt-S3** doped **m-TPAPy** film whose root-mean-square (rms) is 1.168 nm, being lower than those of **m-TPAPy** films doped with **tetra-Pt-N** (1.801 nm), **tetra-Pt-S1** (2.139 nm), **tetra-Pt-S2** (1.964 nm), indicating that the larger steric bulk of the xanthene fragment may more effectively prevent the aggregation of **tetra-Pt-S3** molecules during the film formation process, which is of benefit to the performances of the **tetra-Pt-S3: m-TPAPy** device**.** Therefore, in addition to the high PLQY of the **tetra-Pt-S3: m-TPAPy** film, the balanced carrier transporting property and the better film morphology of the EML also attribute to the high performance of the **tetra-Pt-S3: m-TPAPy** device.

The EQE value is mainly determined by PLQY and the out-coupling efficiency for properly designed phosphorescent OLEDs. The out-coupling efficiency is strongly influenced by the

horizontal transition dipole moment of the EML and could be over 40% when the horizontal dipole ratio of EML is approaching unity.[43] In our case, for the **m-TPAPy** OLEDs with **tetra-Pt-N**, **tetra-Pt-S1,** and **tetra-Pt-S3**, the out-coupling efficiencies are respectively 21.88, 22.30, and 21.26%, estimated by maximum EQE values listed in **Table 3** and corresponding PLQY values shown in **Figure 5**. These out-coupling efficiencies are slightly higher than 20%, indicating that the emission dipoles of **tetra-Pt-N**, **tetra-Pt-S1,** and **tetra-Pt-S3** could be isotropically oriented.[43] For the **tetra-Pt-S2: m-TPAPy** device, on the other hand, its relatively lower EQE is mainly due to the long emission life time of **tetra-Pt-S2.** Compared to the high EQEs of up to 27.6% in vacuum-deposited OLEDs,[26] the EQEs of 14~16% for **tetra-Pt-N** and **tetra-Pt-S1** in solution-processed OLEDs are inferior because of the lower PLQY in the host used, weaker exciton and/or carrier confine ability of the simple device structure, and less orientation of emission dipoles in solution-processed OLEDs.

To further optimize the solution-processed OLEDs with the EML consisting of **tetra-Pt-S3** and **m-TPAPy**, the dopant concentration was changed from 4 to 16 wt%. The device performance data are depicted in **Figure S14** and **S15**, and key parameters of these devices are summarized in **Table 4**. A maximum EQE of 22.4% was achieved at the lowest concentration of 4 wt% and slightly decreased to 21.0% at a high luminance of 1000 cd m^{-1}. These values are comparable and even superior to those of the solution-processed single-cell OLEDs based on phosphorescent Ir(III) and TADF emitters.[7-10, 12-14]

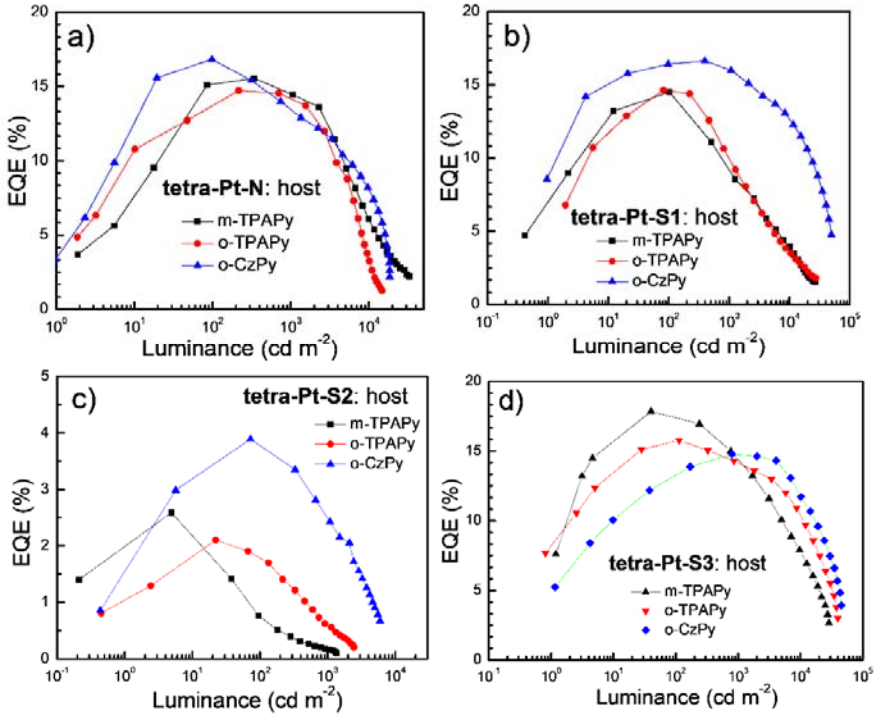

Figure 7. EQE-luminance characteristics of the OLEDs based on a) **tetra-Pt-N**, b) **tetra-Pt-S1**, c) **tetra-Pt-S2,** and d) **tetra-Pt-S3** in different hosts (**m-TPAPy**, **o-TPAPy**, and **o-CzPy**) with a fixed dopant concentration of 12 wt%.

Table 4. Key performance of OLEDs based on **tetra-Pt-S3** in **m-TPAPy**

Concentration [wt%]	L_{max} [cd m^{-2}]	CE [cd A^{-1}]		PE [lm W^{-1}]		EQE [%]		CIE coordinats [x, y]
		Max	at 1000 cd m^{-2}	Max	at 1000 cd m^{-2}	Max	at 1000 cd m^{-2}	
4	37600	77.67	72.84	42.47	39.91	22.39	20.99	0.28, 0.63
8	30300	69.17	61.15	40.04	29.99	19.76	17.48	0.29, 0.63
12	28600	61.62	49.76	35.79	25.30	17.86	14.42	0.31, 0.62
16	33800	47.89	35.29	30.13	16.82	13.65	10.06	0.30, 0.63

CONCLUSION

In summary, we have improved the performance of solution-processed OLEDs based on Pt(II) complexes that has been found to approach to those of state of the art OLEDs based on Ir(III) and TADF emitters. Four tetradentate Pt(II) complexes **tetra-Pt-N**, **tetra-Pt-S1**, **tetra-Pt-S2**, and **tetra-Pt-S3**, were used as the emitter and three organic bipolar materials **m-**

TPAPy, **o-TPAPy**, and **o-CzPy** as the host. By analyzing the PL and EL characteristics of different combinations of the emitters and hosts, we found that **tetra-Pt-S3** gave the best performance among the Pt(II) complexes studied for solution-processed OLEDs. By using **m-TPAPy** as the host, a green-emitting solution-processed **tetra-Pt-S3** OLED with high EQEs of up to 22.4% was realized. More importantly, the EQE roll-off was as low as 6.25% at a high luminance of 1000 cd m^{-2}. We attribute the high performance of the **tetra-Pt-S3**: **m-TPAPy** device to the high k_r/k_{nr} ratio and robust molecular structure of tetra-**Pt-S3** as well as the bipolar transporting property and proper energy levels of **m-TPAPy**.

Experimental Section

Materials: PEDOT:PSS [poly(3,4-ethylenedioxythiophene):poly(styrene sulfonic acid)] (Clevios P AI 4083) was purchased from Heraeus; TmPyPb and TPBi from Luminescence Technology Corp. All of these materials were used as received. **tetra-Pt-N** and **tetra-Pt-S1** were synthesized following the procedure described in ref. 21 in the main text. **m-TPAPy**, **o-TPAPy**, and **o-CzPy** were prepared according to the literature.[30-31] All Pt(II) complexes and organic materials were purified by gradient sublimation prior to use.

Instrumentation and photo-physical measurements: Nuclear magnetic resonance spectra were recorded on DPX-300, 400 and 600 Bruker FT-NMR spectrometer with chemical shifts reported (in ppm) relative to tetramethylsilane (for $CDCl_3$) or non-deuterated solvent residual signal. Unless otherwise stated, all NMR spectra were recorded at room temperature. Mass spectra (FAB and EI) were recorded on a Finnigan MAT 95 mass spectrometer. Elemental analyses were performed at the Institute of Chemistry of the Chinese Academy of Sciences, Beijing. All absorption spectra were recorded on a Hewlett-Packard 8453 diode array spectrophotometer. Steady-state emission spectra were recorded on a SPEX Fluorolog-3 spectrophotometer. Solutions for photo-physical studies were degassed by using a high vacuum

line in a two-compartment cell with five freeze-pump-thaw cycles. Low temperature (77 K) emission spectra for glassy state and solid state samples were recorded in quartz tube (4 mm internal diameter) placed in a liquid nitrogen Dewar flask with quartz windows. The emission quantum yield was measured with $[Ru(bpy)_3](PF_6)_2$ (bpy = 2,2'-bipyridine) in degassed CH_3CN as a standard with $\Phi_{em} = 0.062$ and calculated by: $\Phi_s = \Phi_r(B_r/B_s)(n_s/n_r)^2(D_s/D_r)$, in which the subscripts s and r refer to sample and reference standard solution respectively, n is the refractive index of the solvents, D is the integrated emission intensity and Φ is the luminescence quantum yield. Emission quantum yields of thin film samples were measured with Hamamatsu Quantaurus-QY Absolute PL quantum yields measurement system C11347. Emission lifetime measurements were performed on a Quanta Ray GCR 150-10 pulsed Nd:YAG laser system. Errors for λ values (±1 nm), τ (±10 %), and Φ (± 10 %) are estimated. Nanosecond time-resolved transient absorption and emission measurements were performed on a LP920-KS Laser Flash Photolysis Spectrometer (Edinburgh Instruments Ltd., Livingston, U.K.). The excitation source was the 355 nm output (third harmonic) of a Nd:YAG laser (Spectra-Physics Quanta-Ray Lab-130 Pulsed Nd:YAG laser). The signals were processed by a PC plug-in controller with L900 software. The preparation of samples for the measurements was the same as that for steady-state emission measurements.

Substrate cleaning: Glass slides with pre-patterned ITO electrodes used as substrates of OLEDs were cleaned in an ultrasonic bath of Decon 90 detergent and deionized water, and rinsed with deionized water. Then they were cleaned in sequential ultrasonic baths of deionized water, acetone, and isopropanol, and subsequently dried in an oven for 1 h.

Fabrication and characterization of devices: PEDOT:PSS were spin-coated onto the cleaned ITO-coated glass substrate and baked at 120 ˚C for 20 min to remove the residual water solvent in a clean room. Blends of host materials and Pt(II) complexes were spin-coated from

chlorobenzene atop the PEDOT:PSS layer inside a N_2-filled glove box. The thickness for all EMLs was approximately 60 nm. Afterwards, all devices were annealed at 70 ˚C for 60 min inside the glove box and subsequently transferred into a Kurt J. Lesker SPECTROS vacuum deposition system without exposure to air. Finally, TmPyPb (10 nm), TPBi (40 nm), LiF (1.2 nm), and Al (150 nm) were deposited in sequence by thermal evaporation at a pressure of 10^{-8} mbar. EL spectra, luminance, and CIE coordination were measured by a Photo Research Inc PR-655. Voltage-current characteristics were measured by using a Keithley 2400 source-meter measurement unit. All devices were characterized at room temperature without encapsulation. EQE and power efficiency were calculated by assuming a Lambertian distribution.

ASSOCIATED CONTENT

Supporting Information.

The following files are available free of charge.

Synthetic procedure of **tetra-Pt-S2** and **tetra-Pt-S3**; thermogravimetric analysis (TGA) of **tetra-Pt-2** and **tetra-Pt-3**; energy levels of the bipolar organic molecules; radiative decay and non-radiative decay rate constants of Pt(II) complexes; time-resolved emission spectra of Pt(II) complexes; crystal data of **tetra-Pt-S2**; PL spectra of tetradentate Pt(II) complexes in thin films; EL characteristics of Pt-OLEDs. (PDF)

AUTHOR INFORMATION

Corresponding Author

* E-mail: cmche@hku.hk (C.-M. C.)

* E-mail: clyang@whu.edu.cn (C.-L. Y.)

Notes

The authors declare no competing financial interest.

ACKNOWLEDGMENT

This work was supported by the Innovation and Technology Fund (ITS/224/17FP) and Hong Kong Research Grants Council, General Research Fund (17330416), the Basic Research Program of Shenzhen (JCYJ20160229123546997, JCYJ20170818141858021 and JCYJ20180508162429786) and the National Key Basic Research Program of China (2013CB834802).

REFERENCES

1. Burroughes, J. H.; Bradley, D. D. C.; Brown, A. R.; Marks, R. N.; Mackay, K.; Friend, R. H.; Burns, P. L.; Holmes, A. B., Ligh-emitting diodes based on conjugated polymers. *Nature* **1990,** *347*.
2. de Mello, J. C.; Wittmann, H. F.; Friend, R. H., An improved experimental determination of external photoluminescence quantum efficiency. *Adv. Mater.* **1997,** *9*, 230-232.
3. Kim, J.-S.; Lu, L.; Sreearunothai, P.; Seeley, A.; Yim, K.-H.; Petrozza, A.; Murphy, C. E.; Beljonne, D.; Cornil, J.; Friend, R. H., Optoelectronic and charge transport properties at organic−organic semiconductor interfaces: comparison between polyfluorene-based polymer blend and copolymer. *J. Am. Chem. Soc.* **2008,** *130*, 13120-13131.
4. Snedden, E. W.; Cury, L. A.; Bourdakos, K. N.; Monkman, A. P., High photoluminescence quantum yield due to intramolecular energy transfer in the Super Yellow conjugated copolymer. *Chem. Phys. Lett.* **2010,** *490*, 76-79.
5. Friend, R. H.; Gymer, R. W.; Holmes, A. B.; Burroughes, J. H.; Marks, R. N.; Taliani, C.; Bradley, D. D. C.; Santos, D. A. D.; Bredas, J. L.; Logdlund, M.; Salaneck, W. R., Electroluminescence in conjugated polymers. *Nature* **1999,** *397*, 121-128.
6. Muller, C. D.; Falcou, A.; Reckefuss, N.; Rojahn, M.; Wiederhirn, V.; Rudati, P.; Frohne, H.; Nuyken, O.; Becker, H.; Meerholz, K., Multi-colour organic light-emitting displays by solution processing. *Nature* **2003,** *421*, 829-833.
7. Huang, T.; Jiang, W.; Duan, L., Recent progress in solution processable TADF materials for organic light-emitting diodes. *J. Mater. Chem. C* **2018,** *6*, 5577-5596.
8. Jeon, S. K.; Park, H.-J.; Lee, J. Y., Highly efficient soluble blue delayed fluorescent and hyperfluorescent organic light-emitting diodes by host engineering. *ACS Appl. Mater. Interfaces* **2018,** *10*, 5700-5705.
9. Cai, X.; Chen, D.; Gao, K.; Gan, L.; Yin, Q.; Qiao, Z.; Chen, Z.; Jiang, X.; Su, S.-J., "Trade-Off" hidden in condensed state solvation: multiradiative channels design for highly efficient solution-processed purely organic electroluminescence at high brightness. *Adv. Funct. Mater.* **2018,** *28*, 1704927.
10. To, W.-P.; Zhou, D.; Tong, G. S. M.; Cheng, G.; Yang, C.; Che, C.-M., Highly luminescent pincer gold(III) aryl emitters: thermally activated delayed fluorescence and solution-processed OLEDs. *Angew. Chem. Int. Ed.* **2017,** *56*, 14036-14041.
11. Chiba, T.; Pu, Y.-J.; Kido, J., Solution-processed white phosphorescent tandem organic light-emitting devices. *Adv. Mater.* **2015,** *27*, 4681-4687.

12. Cai, M.; Xiao, T.; Hellerich, E.; Chen, Y.; Shinar, R.; Shinar, J., High-efficiency solution-processed small molecule electrophosphorescent organic light-emitting diodes. *Adv. Mater.* **2011,** *23*, 3590-3596.
13. Zhang, B.; Tan, G.; Lam, C. S.; Yao, B.; Ho, C. L.; Liu, L.; Xie, Z.; Wong, W. Y.; Ding, J.; Wang, L., High-efficiency single emissive layer white organic light-emitting diodes based on solution-processed dendritic host and new orange-emitting iridium complex. *Adv. Mater.* **2012,** *24*, 1873-7.
14. Zou, J.; Wu, H.; Lam, C.-S.; Wang, C.; Zhu, J.; Zhong, C.; Hu, S.; Ho, C.-L.; Zhou, G.-J.; Wu, H.; Choy, W. C. H.; Peng, J.; Cao, Y.; Wong, W.-Y., Simultaneous optimization of charge-carrier balance and luminous efficacy in highly efficient white polymer light-emitting devices. *Adv. Mater.* **2011,** *23*, 2976-2980.
15. Di, D.; Romanov, A. S.; Yang, L.; Richter, J. M.; Rivett, J. P. H.; Jones, S.; Thomas, T. H.; Abdi Jalebi, M.; Friend, R. H.; Linnolahti, M.; Bochmann, M.; Credgington, D., High-performance light-emitting diodes based on carbene-metal-amides. *Science* **2017,** *356*, 159-163.
16. Jou, J.-H.; Sahoo, S.; Dubey, D. K.; Yadav, R. A. K.; Swayamprabha, S. S.; Chavhan, S. D., Molecule-based monochromatic and polychromatic OLEDs with wet-process feasibility. *J. Mater. Chem. C* **2018,** *6*, 11492-11518.
17. Liu, B.; Dang, F.; Tian, Z.; Feng, Z.; Jin, D.; Dang, W.; Yang, X.; Zhou, G.; Wu, Z., High triplet energy level achieved by tuning the arrangement of building blocks in phosphorescent polymer backbones for furnishing high electroluminescent performances in both blue and white organic light-emitting devices. *ACS Appl. Mater. Interfaces* **2017,** *9*, 16360-16374.
18. Wang, S.; Yang, Q.; Zhang, B.; Zhao, L.; Xia, D.; Ding, J.; Xie, Z.; Wang, L., Improving the power efficiency of solution-processed phosphorescent WOLEDs with a self-host blue iridium dendrimer. *Adv. Opt. Mater.* **2017,** *5*, 1700514.
19. Sarada, G.; Cho, W.; Maheshwaran, A.; Sree, V. G.; Park, H.-Y.; Gal, Y.-S.; Song, M.; Jin, S.-H., Deep-Blue phosphorescent ir(III) complexes with light-harvesting functional moieties for efficient blue and white pholeds in solution-process. *Adv. Funct. Mater.* **2017,** *27* , 1701002.
20. Jou, J.-H.; Fu, S.-C.; An, C.-C.; Shyue, J.-J.; Chin, C.-L.; He, Z.-K., High efficiency yellow organic light-emitting diodes with a solution-process feasible iridium based emitter. *J. Mater. Chem. C* **2017,** *5*, 5478-5486.
21. Yang, X.; Guo, H.; Liu, B.; Zhao, J.; Zhou, G.; Wu, Z.; Wong, W.-Y., Diarylboron-based asymmetric red-emitting ir(III) complex for solution-processed phosphorescent organic light-emitting diode with external quantum efficiency above 28%. *Adv. Sci.* **2018,** *5*, 1701067.
22. Han, T.-H.; Choi, M.-R.; Jeon, C.-W.; Kim, Y.-H.; Kwon, S.-K.; Lee, T.-W., Ultrahigh-efficiency solution-processed simplified small-molecule organic light-emitting diodes using universal host materials. *Sci. Adv.* **2016,** *2*, e1601428
23. Baldo, M. A.; O'Brien, D. F.; You, Y.; Shoustikov, A.; Sibley, S.; Thompson, M. E.; Forrest, S. R., Highly efficient phosphorescent emission from organic electroluminescent devices. *Nature* **1998,** *395*, 151-154.
24. Kui, S. C. F.; Chow, P. K.; Tong, G. S. M.; Lai, S.-L.; Cheng, G.; Kwok, C.-C.; Low, K.-H.; Ko, M. Y.; Che, C.-M., Robust Phosphorescent platinum(II) complexes containing tetradentate O^N^C^N ligands: excimeric excited state and application in organic white-light-emitting diodes. *Chem. Eur. J.* **2013,** *19*, 69-73.
25. Cheng, G.; Chow, P.-K.; Kui, S. C. F.; Kwok, C.-C.; Che, C.-M., High-efficiency polymer light-emitting devices with robust phosphorescent platinum(ii) emitters containing tetradentate dianionic O^N^C^N ligands. *Adv. Mater.* **2013,** *25*, 6765-6770.

26. Cheng, G.; Kui, S. C. F.; Ang, W.-H.; Ko, M.-Y.; Chow, P.-K.; Kwong, C.-L.; Kwok, C.-C.; Ma, C.; Guan, X.; Low, K.-H.; Su, S.-J.; Che, C.-M., Structurally robust phosphorescent [Pt(O^N^C^N)] emitters for high performance organic light-emitting devices with power efficiency up to 126 lm W^{-1} and external quantum efficiency over 20%. *Chem. Sci.* **2014,** *5*, 4819-4830.
27. Cheng, G.; Chen, Y.; Yang, C.; Lu, W.; Che, C.-M., Highly efficient solution-processable organic light-emitting devices with pincer-type cyclometalated platinum(II) arylacetylide complexes. *Chem. Asian J.* **2013,** *8*, 1754-1759.
28. Yang, X.; Froehlich, J. D.; Chae, H. S.; Harding, B. T.; Li, S.; Mochizuki, A.; Jabbour, G. E., Efficient Light-Emitting Devices Based on Platinum-Complexes-Anchored Polyhedral Oligomeric Silsesquioxane Materials. *Chem. Mater.* **2010,** *22* (16), 4776-4782.
29. Yang, X.; Jiao, B.; Dang, J.-S.; Sun, Y.; Wu, Y.; Zhou, G.; Wong, W.-Y., Achieving high-performance solution-processed orange OLEDs with the phosphorescent cyclometalated trinuclear Pt(II) complex. *ACS Appl. Mater. Interfaces* **2018,** *10*, 10227-10235.
30. Su, S.-J.; Sasabe, H.; Takeda, T.; Kido, J., Pyridine-containing bipolar host materials for highly efficient blue phosphorescent OLEDs. *Chem. Mater.* **2008,** *20*, 1691-1693.
31. Gong, S.; Chen, Y.; Yang, C.; Zhong, C.; Qin, J.; Ma, D., De novo design of silicon-bridged molecule towards a bipolar host: all-phosphor white organic light-emitting devices exhibiting high efficiency and low efficiency roll-off. *Adv. Mater.* **2010,** *22*, 5370-5373.
32. Gong, S.; Chen, Y.; Luo, J.; Yang, C.; Zhong, C.; Qin, J.; Ma, D., Bipolar tetraarylsilanes as universal hosts for blue, green, orange, and white electrophosphorescence with high efficiency and low efficiency roll-off. *Adv. Funct. Mater.* **2011,** *21*, 1168-1178.
33. Gong, S.; Fu, Q.; Wang, Q.; Yang, C.; Zhong, C.; Qin, J.; Ma, D., Highly efficient deep-blue electrophosphorescence enabled by solution-processed bipolar tetraarylsilane host with both a high triplet energy and a high-lying homo level. *Adv. Mater.* **2011,** *23*, 4956-4959.
34. Nakanotani, H.; Higuchi, T.; Furukawa, T.; Masui, K.; Morimoto, K.; Numata, M.; Tanaka, H.; Sagara, Y.; Yasuda, T.; Adachi, C., High-efficiency organic light-emitting diodes with fluorescent emitters. *Nat. Commun.* **2014,** *5*, 4016.
35. Gong, X.; Ma, W.; Ostrowski, J. C.; Bazan, G. C.; Moses, D.; Heeger, A. J., White electrophosphorescence from semiconducting polymer blends. *Adv. Mater.* **2004,** *16*, 615-619.
36. Gu, Y.; Zhu, L.; Jin, Y.; Li, Y.; Gong, S.; Ma, D.; Qin, J.; Yang, C., Synthesis and properties of pyridine-containing bipolar host materials for blue phosphorescent OLEDs. *Sci. China-Chem.* **2013,** *43*, 472.
37. Zhou, M.; Wang, P.; Zhang, Z.; Huang, H., Bipolar blue-phosphorescence material, preparation method thereof and organic electroluminescent device. *CN 104017566 A* **2014**.
38. Williams, J. A. G.; Beeby, A.; Davies, E. S.; Weinstein, J. A.; Wilson, C., An alternative route to highly luminescent platinum(II) complexes: cyclometalation with N^C^N-coordinating dipyridylbenzene ligands. *Inorg. Chem.* **2003,** *42*, 8609-8611.
39. Kwok, C.-C.; Ngai, H. M. Y.; Chan, S.-C.; Sham, I. H. T.; Che, C.-M.; Zhu, N., [(O^N^N)PtX] complexes as a new class of light-emitting materials for electrophosphorescent devices. *Inorg. Chem.* **2005,** *44*, 4442-4444.
40. Chen, Y.; Li, K.; Lu, W.; Chui, S. S.-Y.; Ma, C.-W.; Che, C.-M., Photoresponsive supramolecular organometallic nanosheets induced by Pt(II)···Pt(II) and C-H···π interactions. *Angew. Chem. Int. Ed.* **2009,** *48*, 9909-9913.
41. Poriel, C.; Rault-Berthelot, J., Structure-property relationship of 4-substituted-spirobifluorenes as hosts for phosphorescent organic light emitting diodes: an overview. *J. Mater. Chem. C* **2017,** *5*, 3869-3897.

42. Kui, S. C. F.; Chow, P. K.; Cheng, G.; Kwok, C.-C.; Kwong, C. L.; Low, K.-H.; Che, C.-M., Robust phosphorescent platinum(II) complexes with tetradentate O^N^C^N ligands: high efficiency OLEDs with excellent efficiency stability. *Chem. Commun.* **2013,** *49*, 1497-1499.
43. Kim S.-Y.;, Jeong, W.-I.; Mayr, C.; Park, Y.-S.; Kim, K.-H.; Lee, J.-H.; Moon, C.-K.; Brütting, W.; Kim, J.-J., Organic Light-Emitting Diodes with 30% External Quantum Efficiency Based on a Horizontally Oriented Emitter. *Adv. Funct. Mater.* **2013**, *23*, 3896-3900.